arXiv:2309.11685v1 [cond-mat.mes-hall] 20 Sep 2023

Topological Floquet Flat Bands in Irradiated Alternating Twist Multilayer Graphene

Yingyi, Huang[1, *]

[1] *School of Physics and Optoelectronic Engineering, Guangdong University of Technology, Guangzhou 510006, China*

(Dated: September 22, 2023)

We study the appearance of topological Floquet flat bands in alternating-twist multilayer graphene (ATMG) which has alternating relative twist angle $\pm\theta$ near the first magic angle. While the system hosts both flat bands and a steep Dirac cone in the static case, the circularly polarized laser beam can open a gap at the Moiré K point and create Floquet flat bands carrying non-zero Chern numbers. Considering the recent lattice-relaxation results, we find that the topological flat band is well-isolated for the effective interlayer tunneling in $n = 3, 4, 5$ layer. Such dynamically produced topological flat bands are potentially observed in the experiment and thus provide a feasible way to realize the fractional Chern insulator.

I. INTRODUCTION

Recent progress of twisted bilayer graphene (TBG) puts the graphene back to the center of condensed matter physics because of the discovery of strong correlation and superconductivity in such system [1–3]. These exotic phenomena appear to be related to the presence of flat bands, which is a result of the flattening of Dirac cones at certain special twist angles, called magic angles [4, 5]. Around charge neutrality, interaction effects are enhanced by van Hove singularities coming from the nearly flat bands at these magic angles. On the other hand, the flat bands in twist bilayer graphene are generally topologically nontrivial even in the absence of spin-orbit coupling [6–10]. A lot of studies were done to explore the topological feature in the mini Brillouin zone from the large Moiré superlattice [6–8, 11]. These narrow enough topological flat bands are particularly relevant to various exotic fractional quantum Hall effect [12–15]. However, the small magic angle and coupling ratio between intra-sublattice and inter-sublattice hopping parameters make the realization of a fractional Chern insulator in TBG remains elusive.

Recently, people have turned their attention to multilayer graphene systems [16–21]. For example, alternating-twist multilayer graphene (ATMG) is a promising platform to realize phases seen in TBG [17, 22–26], in which the nearest neighboring layers are aligned and have alternating relative twists of $\pm\theta$. Remarkably, it can be mapped exactly to a sequence of decoupled twisted bilayer graphene subsystems (plus single-layer graphene) for an odd (even) number of layers [27–29]. Topological phases not only have been experimentally observed in other multilayer systems, including ABC trilayer graphene on a hexagonal boron nitride [30–34] and twisted double-bilayer graphene [35–38], they also have been found in ATMG under in-plane magnetic field and out of plane electric field [27]. However, it is found that after decoupling mapping the intra-subsystem action of the electromagnetic fields vanishes in odd-layer ATMG or decays with increasing layer number in even-layer ATMG [27]. To adjust the intra-subsystem coupling, it is necessary to utilize other experimental techniques.

Optical engineering of the physical properties of a solid is a highly controllable method. In particular, strong circularly polarized light driving opens the gap between bands by periodically changing the Hamiltonian and can be described by Floquet theory [39–49]. Its application can be dated back to the utilize photon to open the gap in the Haldane model [50]. Furthermore, the Floquet method on twisted bilayer graphene can make the low-energy flat band becomes topological [51–55]. Thus, it is worthwhile to investigate ATMG under the driving of circularly polarized light.

In this paper, we study the effect of circularly polarized light on ATMG. Interestingly, we find that, under the high-frequency limit, irradiated ATMG can be decomposed to irradiated bilayer subsystems (irradiated single layer), as illustrated in Fig. 1). This mapping is similar to those with an electric field or a magnetic field [27–29], but there is no decay factor rescaling the light field. In particular, despite the existence of a Dirac cone at K_M point, the light field induces gap opening and isolates the central Floquet band (see Fig. 2), and thus changes the topology of the flat band. The model is given in Sec. II and the mapping is presented in Sev. III. In Sec. IV, we calculate the Floquet band spectrum in trilayer graphene and show the existence of the Floquet topological flat band. The numerical results for $n = 4, 5$ layers are presented in Sec.V. Since the ratio between the same-sublattice and opposite-sublattice hopping $u = w_0/w_1$ is layer dependent and sensitive to lattice-relaxation in ATMG [27, 56], we check the existence of Floquet topological flat band at the first magic angle and its corresponding effective u in different layers. The advantages of the Floquet method on ATMG are addressed in the conclusion part in Sec. VI.

* yyhuang@gdut.edu.cn

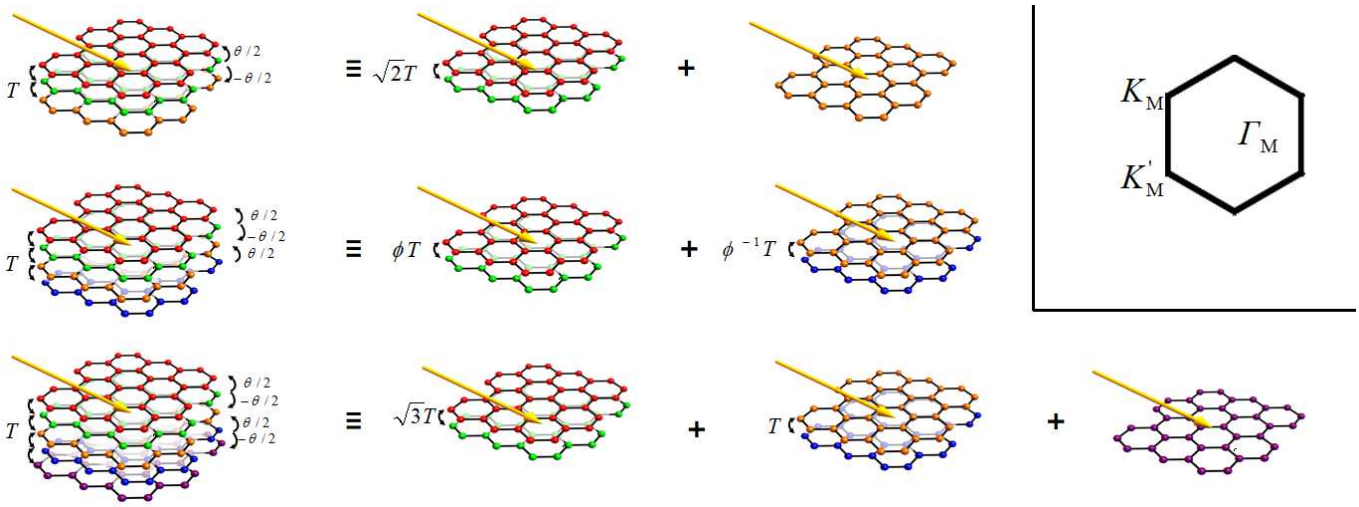

FIG. 1. Illustration of decomposition of ATMG irradiated by circularly polarized light $\mathbf{A}(t) = A(\cos\Omega t, \sin\Omega t)$ into TBG and graphene subsystems for $n = 3, 4, 5$ layers. For $n = 4$, the inter-subsystem coupling ratio is $\phi = \frac{1+\sqrt{5}}{2}$ and its inverse. The terms generated by the light field act within subsystems. Inset: The Moire Brillouin zone.

II. MODEL

Now we consider a general system of $n-$layer ATMG irradiated by a beam of circularly polarized light. The relative twist between two neighboring layers has the same magnitude but alters in sign ($\pm\theta$). Here, the relative displacement is neglected since the zero shift configuration is energetically favorable [27]. The electromagnetic vector potential of the light is given by $\mathbf{A}(t) = A(\cos\Omega t, \sin\Omega t)$ with t being the time, Ω being the frequency, A being the field strength. The multiplication of Ω and A is the electric field amplitude, $E = \Omega A$.

The low-energy physics of the system for one of the valleys can be modeled by

$$H(t) = \begin{bmatrix} h_{\theta/2}(t) & T & 0 & \cdots \\ T^\dagger & h_{-\theta/2}(t) & T^\dagger & \cdots \\ 0 & T & h_{\theta/2}(t) & \cdots \\ \cdots & \cdots & \cdots & \cdots \end{bmatrix}, \qquad (1)$$

where $h_{\theta/2}(t) = v_F[-i\hbar\boldsymbol{\nabla} - e\mathbf{A}(t)] \cdot \boldsymbol{\sigma}_{\theta/2}$, with rotated Pauli matrices $\boldsymbol{\sigma}_{\theta/2} \equiv e^{-i\theta\sigma_z/4}(\sigma_x, \sigma_y)e^{i\theta\sigma_z/4}$ and Fermi velocity v_F, is the low-energy Dirac Hamiltonian of a valley of a single graphene sheet twisted by angle $\theta/2$. The time-dependent electromagnetic potential $\mathbf{A}(t)$ is introduced into the Hamiltonian by way of minimal substitution. The interlayer tunneling matrix $T = \sum_{n=1}^{3} T_n e^{-ik_\theta \mathbf{q}_n \cdot \mathbf{r}}$, with

$$T_n = w_{AA}\sigma_0 + w_{AB}\mathbf{q}_n \cdot \boldsymbol{\sigma}_{\pi/2}, \qquad (2)$$

where the unit vectors $\mathbf{q}_1 = (0, -1)$, $\mathbf{q}_{2,3} = (\pm\sqrt{3}/2, 1/2)$ encode the tunneling w_{AA} and w_{AB} between the AA- and AB-stacked regions of the twisted bilayer graphene. $k_\theta = 8\pi\sin(\theta/2)/3a$ is the wavevector of the Moiré pattern and a is the Bravais lattice spacing of graphene.

In the Floquet theory, the periodically changed vector potential modifies the static Hamiltonian to $H_{\mathbf{k}}(t) = H_{\mathbf{k}}(t + T)$. One focuses on quasienergies $\epsilon_{\mathbf{k}s}$, and periodically changed Floquet modes $|\phi_{\mathbf{k}s}(t)\rangle = |\phi_{\mathbf{k}s}(t + T)\rangle$, where T is the period and $\mathbf{k}$ is the crystal momentum, by solving the Floquet-Schrödinger equation $[H_{\mathbf{k}}(t) - i\hbar\partial_t]|\phi_{\mathbf{k}s}(t)\rangle = \epsilon_{\mathbf{k}s}|\phi_{\mathbf{k}s}(t)\rangle$. The quasienergies fall into a so-called "Floquet zone" with size $\hbar\Omega$ similar to the concept of the Brillouin zone but in the time dimension. The relation between Floquet modes $|\phi_{\mathbf{k}s}(t)\rangle$ and the wave function governed by the time-dependent Schrödinger equation $|\phi_{\mathbf{k}s}(t)\rangle$ is $|\phi_{\mathbf{k}s}(t)\rangle \equiv e^{i\epsilon_{\mathbf{k}s}t/\hbar}|\psi_{\mathbf{k}s}(t)\rangle$.

The simulation parameters are chosen from the experimentally known electronic structure [57] as follows: $a = 2.4$ Å, $\hbar v_F/a = 2.425$ eV, and $w_{AB} = 112$ meV . Correspondingly, $\alpha \equiv w_{AB}/\hbar v_F k_\theta = 1.1 \times 10^{-2}/2\sin(\theta/2)$ is a function of the twist angle θ. Throughout this paper, the laser parameters are chosen to be $A = 0.08a^{-1}$ and $\Omega = 6eV/\hbar$ which are experimentally attainable.

The interlayer tunneling around the magic angle is affected by atomic relaxation. Especially, this relaxation effect becomes stronger with the number of layers being increased [27, 58]. The relaxation of atoms in multilayer geometry will decrease the interlayer distance at AB stacking and increase the one at AA stacking. This reduces the AA tunneling w_0 and increases the AB tunneling w_1, and thus changing their ratio $u = w_0/w_1$. In trilayer graphene ($n = 3$), the first principle calculation gives the value of the first magic angle $\theta = 1.49°$ and the effective $u = 0.585$. For $n = 4, 5$, the distinction between tunneling at inner and outer interfaces changes the value of the magic angle. For $n = 4$, the value of the first magic angle is $\theta = 1.68°$ and the effective $u = 0.614$. For $n = 5$, the second magic angle is within reach. The value of the first and second magic angles are $\theta = 1.79°$ and $\theta = 1.14°$, and the corresponding effective u are 0.627

and 0.45 [27].

III. THE REDUCTION OF EFFECTIVE HAMILTONIAN IN THE HIGH-FREQUENCY LIMIT

In the high-frequency limit, light does not directly excite electrons and instead effectively modifies the electron band structures. Its influence can be represented by an effective static Hamiltonian $\Delta H_F = i\hbar/T \log U$, where $U = \mathcal{T}\exp[-i/\hbar \int_0^T H(t)dt]$ is the time-evolution operator, with $\mathcal{T}$ being the time-ordering operator. For $A^2 \ll 1$, we can consider the $\delta H_F = [H^{(-1)}, H^{(1)}]/\hbar\Omega$. Here, $H^{(n)} = \int_0^1 e^{-2\pi i n\tau} H(2\pi\tau/\Omega)d\tau$ for $n = 0, 1, 2, \cdots$ are the Fourier components of the periodic Hamiltonian.

Now we have the effective Hamiltonian $H_F = H^{(0)} + \delta H_F$, where $H^{(0)}$ the static part with A being set to zero and the modification part being

$$\delta H_F = B(\mathbb{1} \otimes \sigma_z). \tag{3}$$

Here, $B = \frac{(ev_F A)^2}{\hbar\Omega}$ and $\mathbb{1}$ is an n-dimensional identity matrices for a n-layer system. σ_z is a Pauli matrix acting on the individual layer's A and B sublattice degree-of-freedom, and thus breaks time-reversal symmetry.

Following a similar procedure in static systems [28], we continue to decompose the effective Hamiltonian H_F for $n = 3, 4, 5$ layers irradiated ATMG using a unitary transformation. The transformation V is a $2n$-dimensional transformation matrix, which is given in Refs. 28 and 56. Using the unitary transformation on the static part and the modification part of H_F separately, we have $V^T(H^{(0)} + \delta H_F)V = V^T H^{(0)} V + V^T \delta H_F V$.

After the transformation, the static Hamiltonian generates a TBG subsystem $\mathcal{H}_1$. For different layers of ATMG, the remaining subsystems $\mathcal{H}_2, \mathcal{H}_3, \cdots$ that arise from the static Hamiltonian can be graphene, non-TBG, or their combinations. For the modification part, since V is independent of the sublattices, the transformation leaves δH_F unchanged. That is, $V^T \delta H_F V = \delta H_F$. From the fact that the modification parts can be written as a direct sum of σ_z terms, $\delta H_F = B(\sigma_z \oplus \sigma_z \oplus \cdots)$, we have

$$H^{dec} = (\mathcal{H}_1 + B\sigma_0 \otimes \sigma_z) \oplus (\mathcal{H}_2 + B\sigma_0 \otimes \sigma_z) \oplus \cdots . \tag{4}$$

For TBG, the corresponding term becomes $\mathcal{H}_i + B\sigma_0 \otimes \sigma_z$. For single-layer graphene, the corresponding term becomes $\mathcal{H}_i + B\sigma_z$. From Eq. 4, the effect of a beam of circularly polarized light on the ATMG can be presented by multiple independent beams of circularly polarized light on each subsystem, as shown in Fig. 1.

One of the remarkable consequences is that the δH_F modifies the low-energy electron band structure. To illustrate the effect of light, we consider a 3-layer ATMG as shown in Fig. 2. We focus on the two lowest positive energy bands. For static bands ($E's$), while the lowest one (E_1) is a flat band in the TBG subsystem, the second one from the other subsystem (E_2) hosts a Dirac cone at the K_M point. The effect of light on the two subsystems can be shown by the shifts of the two lowest Floquet energy levels ($\epsilon's$). Actually, as evident in Fig. 2, the gap openings in the low-energy subsystems at K_M point isolate the central Floquet band ϵ_1. The band gap between the positive and negative central Floquet bands ϵ_{1g} is nonzero and is twice the distance between ϵ_1 and zero energy $\epsilon_{1g}/2 = E_{1g}/2 + \Delta_1$, with Δ_1 being the gap opening of the lower energy level in TBG subsystem. For the band gap above the positive central Floquet band ϵ_{2g}, we should discuss $u = 0$ and $u > 0$ cases separately. In the chiral limit ($u = 0$), the static bands E_1 and E_2 touch each other at zero energy, i.e., $E_{1g} = 0$. The Floquet band gap $\epsilon_{2g} = \Delta_2 - \Delta_1$. The shift of the Dirac cone under $B\sigma_z$ term is $\Delta_2 = B$. Δ_1 can be calculated from the eigenenergies of δH_F as B. Thus, the ϵ_{2g} gap keeps closing at K_M points for $u = 0$. In contrast, for $u > 0$, $\epsilon_{2g} = \Delta_2 - \Delta_1 - E_{1g}/2$. Δ_2 is independent of u and always equal to B. In TBG system, $\epsilon_{1g} = 2\Delta_1 + E_{1g}$ is always smaller than the value at zero u [51] which means $\epsilon_{1g} < B$. Therefore, for finite u, $\Delta_1 + E_{1g}/2$ is smaller than Δ_2 and leads to the opening of gap ϵ_{2g}.

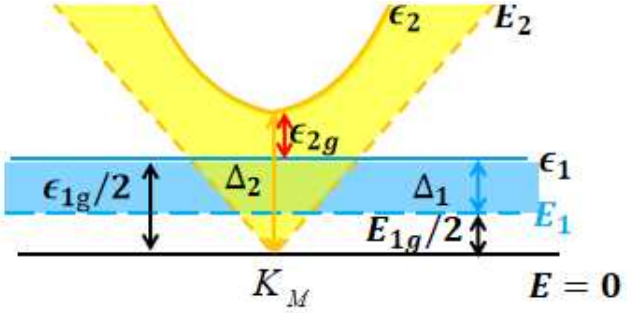

FIG. 2. The schematics of low-energy band structure of $n = 3$ ATMG near K_M point at a magic angle. The static (Floquet) bands $E's$ ($\epsilon's$) are represented by dashed (solid) lines. The first (second) lowest energy level E_1 and ϵ_1 (E_2 and ϵ_2) in blue (yellow) are from the TBG (graphene) subsystem. The gap opening of the first (second) lowest energy level at K_M point is marked by the blue (yellow) region $\Delta_{1(2)} = \epsilon_{1(2)} - E_{1(2)}$. The distance from the lowest static (Floquet) bands to zero energy is denoted by $E_{1g}/2$ ($\epsilon_{1g}/2$). The gap between the two static (Floquet) bands is denoted by E_{2g} (ϵ_{2g}).Note that particle-hole asymmetry is not considered here.

From the above analysis, we can see that the circularly polarized light on the ATMG opens the gaps ϵ_{1g} and ϵ_{2g} at K_M point and isolate the flat band with $u > 0$. This can be generalized to ATMG with $n > 3$.

IV. THE TRILAYER CASE ($n = 3$)

In order to check the isolation of the central Floquet band, we now examine the $n = 3$ ATMG Floquet spectrum numerically.

The Floquet spectrum can be calculated numerically by the Hamiltonian Eq. 1 via the Floquet-Schrödinger

approach. The Floquet spectrum shown in Fig. 3(a) is at the first magic angle and the corresponding tunneling ratio chosen from the lattice relaxation result. The spectrum exhibits apparent electron-hole asymmetry due to the relaxation [10]. Similar to the TBG case, the hole side gets much wider than the electron side. The positive (negative) central Floquet energy bands $\epsilon_{1+(-)}$ corresponds to the lower band of the TBG subsystem. And the Floquet band next to the central one $\epsilon_{2+(-)}$ corresponds to the graphene subsystem and hosts a steep Dirac cone at K_M point, which is absent in TBG system.

While the gap opening at K_M point for finite u is proven in the last section, the indirect gap between the minimum value of ϵ_{2+} and the maximal value of ϵ_{1+} is not always opened. Fig. 3(a) shows that the minimal of ϵ_{2+} at Γ_M point is lower than the maximal value of ϵ_{1+} at K_M point, giving a negative indirect gap. Thus, we should use the direct gap instead of the indirect one to characterize the band feature.

A numerical calculation of Chern numbers at $(u, \alpha) = (0.585, 0.425)$ (Fig. 3 (a)) gives a non-trivial topological number ± 4. This can be understood from the fact that time-reversal breaking induces valley and spin degeneracies in the irradiation ATMG system, just similar to the TBG case [51]. In Fig. 3(b), for $(u, \alpha) = (0.5, 0.8024)$, however, a gap closing takes place at the Γ_M points and gives a trivial Chern number. Thus, it is necessary to investigate the band features under different effective interlayer tunneling u and twist angle α.

Now we show the phase diagrams for the bandwidth and band gaps of the central Floquet band. The bandwidth of the two central bands is shown in Fig. 4(a), sharing many similarities to the irradiated TBG. Especially, the irradiated ATMG has advantages over static cases. Firstly, the flat bands exist over a wider range of twist angles. This is true in both two regions: the one around the magic angle ($\alpha = 0.425$) in the whole range of u and the one at $\alpha > 0.425$ and large u. Secondly, the bandwidths of the lowest energy bands in the irradiated case are smaller than those in the static case. This is obvious near the chiral limit ($u < 0.2$) and small twist angle ($\alpha > 0.5$). The most important characteristic of $n = 3$ ATMG is that the flat band regions are at larger twist angles than irradiated TBG. This can be understood from the fact that the magic angle of three-layer ATMG is $\sqrt{2}\theta_{TBG}$, which is larger than the one of TBG.

Before searching the topological region of the flat band, we should find the band isolation regions by calculating the band gaps. The gap ϵ_{1g} can be seen in Fig. 4(b). It becomes smaller with increasing u but remains nonvanishing in the entire regions. This is consistent with the TBG case since the $\epsilon_{1+(-)}$ bands belong to the TBG subsystems.

The situation for the ϵ_{2g} gap is more complicated. Due to the electron-hole asymmetry, the ϵ_{2+g} and ϵ_{2-g} gap for the electron and hole parts are not the same. Fig. 4 (c) exhibits fewer dark regions which correspond to fewer gap closings. This can be understood from the fact that the hole part of the spectrum is wider than the electron part.

For the ϵ_{2-g} gap, we found two gap closings. The first gap closing at K_M point is around the chiral limit $u = 0$, as discussed in Sec. III. As the interlayer tunneling ratio increases, another gap closing appears at Γ_M point for large u, as given in Fig. 3(b). The region between the two gap closing is topological. Remarkably, the flat band at the first magic angle and its corresponding effective interlayer ratio from lattice relaxation calculation falls into this topological region (marked by a red star).

For the positive energy, the phase diagram of ϵ_{2+g} (Fig. 4(d)) exhibits two additional gap closings at Γ_M point for smaller twist angles closing to $u = 1$. They are very close to the gap closings in the TBG case (see Fig.3(b) in Ref. [51]) with a $\sqrt{2}$ amplification factor on the y-axis.

Therefore, although the gap closings at Γ_M point make the phase diagram for $n = 3$ ATMG more complicated, they have no influence on the existence of the topological isolated flat bands at the first magic angle, whose twist angle is larger than the one of TBG.

V. $n = 4, 5$

For an ATMG system with more layers, more subsystems appear after decomposition. We should look at their influences on the central Floquet bandwidth and bandgaps.

According to the discussion in Sec. III, we know that the laser field opens gaps in the TBG subsystem for ATMG with different layer numbers. Most importantly, for ATMG, except the interlayer tunneling, both the laser parameter $B = \frac{(ev_F A)^2}{\hbar\Omega}$ and intralayer tunneling in the TBG subsystem do not depend on the layer number. We expect that the bandwidth $\delta\epsilon_0$ and the band gap ϵ_{1g} phase diagram in Figs. 5(a)(b) and Figs. 6(a)(b) are similar to the bilayer and the trilayer cases.

Actually, the increment of subsystems changes the ϵ_{2g} gap. The ϵ_{2-g} gap for $n = 4$ and $n = 5$ are shown in Fig. 5(c) and Fig. 6(c). As a result of particle-hole asymmetry, ϵ_{2+g} gap is more complicated and is shown in the Fig. 5(d) and Fig. 6(d). For $n = 4$, the ATMG maps to a TBG subsystem and a non-magic TBG subsystem. The non-magic TBG subsystem, which is away from the magic angles, hosts Dirac cones at K_M and K'_M points. When these Dirac cones touch the lowest energy level ϵ_1, they close the band gap ϵ_{2-g}. This is similar to the effect of the Dirac cone of the graphene subsystem in the trilayer system. In Fig. 5(d), we can see that the ϵ_{2+g} gap closing change the phase diagram. However, the ϵ_{2+g} gap at the first magic angle is opened, and thus the central band is topologically nontrivial.

For the $n = 5$ case, there are a non-TBG subsystem and a graphene subsystem besides the TBG subsystem. The appearance of Dirac cones in either the non-magic TBG or the graphene subsystem closes the ϵ_{2g} gap. As

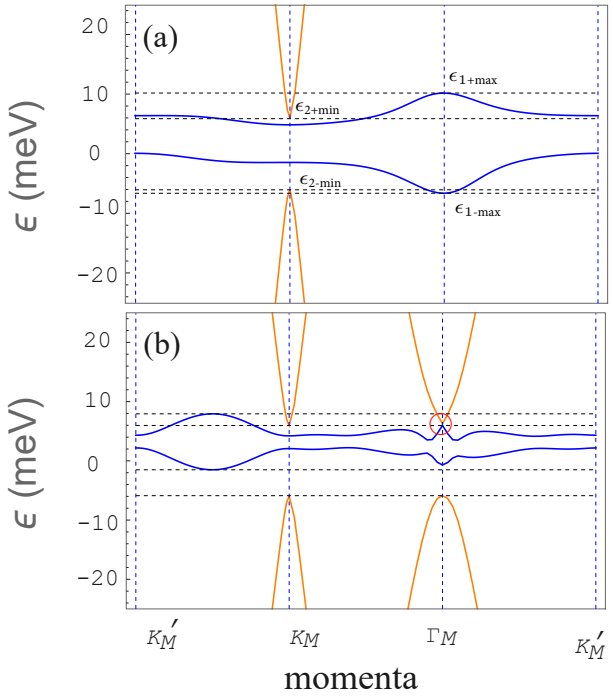

FIG. 3. (a)The band structure of irradiated trilayer ATMG at the first magic angle $\alpha = 0.425$ and the corresponding effective inter-layer tunneling $u = 0.585$, which is pointed out by a red star in Fig. 4(c). The central bands are nontrivial and have Chern number ± 4. (b) The band structure of irradiated trilayer ATMG at a gap closing point $(\alpha, u) = (0.5, 0.8024)$, which is pointed out by a black arrow in Fig. 4(d). The red circle mark the ϵ_{2+g} gap closing, indicating the central band ϵ_{1+} trivial. The laser frequency and electric field are set at $\hbar\Omega = 6eV$ and $E = 2 \times 10^4 kV/cm$.

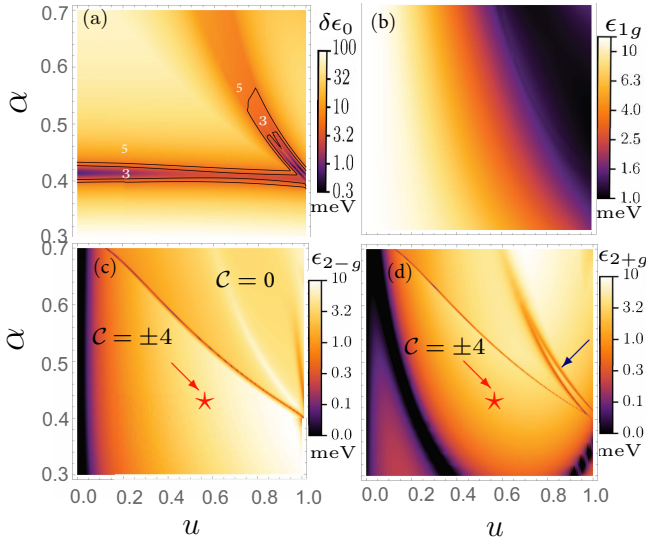

FIG. 4. (a) The bandwidth for the central band ϵ_0, (b) the Floquet band gaps between central bands ϵ_{1g}, (c) the Floquet band gaps between the central negative band and the next band ϵ_{2-g}, (d) the Floquet band gaps between the central positive band and the next band ϵ_{2+g} as a function of twist angle and the ratio of interlayer tunneling u. In (c) and (d), the red star denotes the first magic angle and its corresponding u from lattice relaxation. The laser parameters are the same as in Fig. 3.

a result, a more complicated phase diagram is found in Figs. 6(c) and (d). The bands at the two first magic angles are in the gapped and topological phases.

VI. DISCUSSION AND CONCLUSION

In this paper, we have investigated irradiated alternating-twist multilayer graphene at charge neutral. By mapping the multilayer system into a direct sum of bilayer systems (plus a single-layer system), we have shown that the laser field opens gaps between the central Floquet flat bands and between the ones next to them for $u > 0$. Numerical results of $n = 3, 4, 5$ further show that the gap opening makes the Floquet flat bands topological in certain twist angle and tunneling ratio regions despite the complicated gap closing features at K_M (K'_M) and Γ_M points induced by the coexisting Dirac cones. These findings extend the Floquet study on TBG and other multilayer graphene systems, confirming the existence of topological Floquet flat band in ATMG.

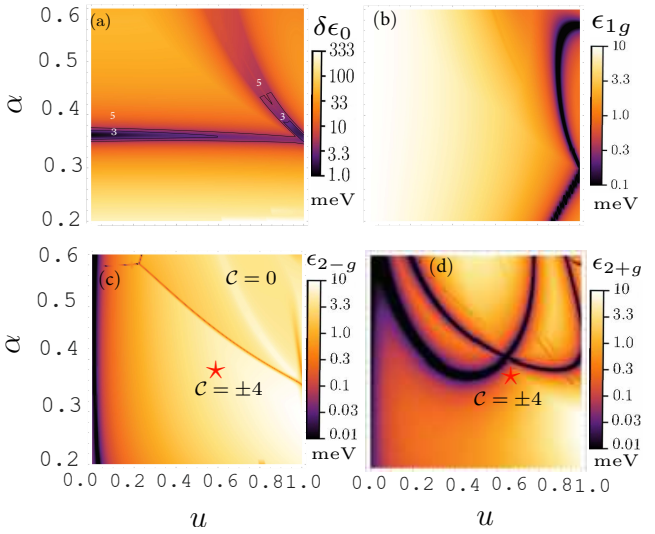

FIG. 5. The bandwidth and the bandgap for $n = 4$ layer. The labels and laser parameters are the same as in Fig. 4.

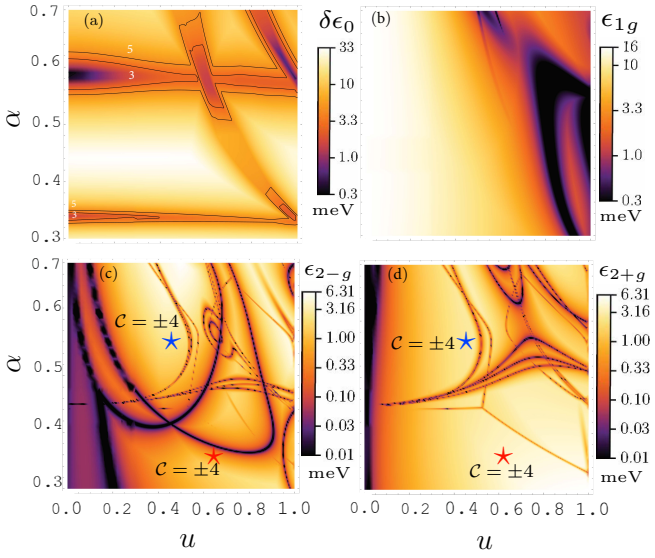

FIG. 6. The bandwidth and the bandgap for $n = 5$ layer. The labels and laser parameters are the same as in Fig. 4. In (c) and (d), the red and blue stars denote the first and the second magic angle and their corresponding u from lattice relaxation.

Floquet engineering ATMG is a promising platform to realize the Floquet fractional Chern insulators, which can be seen in three ways. Firstly, it has advantages over out-of-plane electric fields and in-plane magnetic fields proposed in ATMG. For odd numbers of layers, the electromagnetic fields only act as tunneling terms between different subsystems. For even layers, the electromagnetic fields induce an effective intralayer coupling but the coupling is rescaled by a factor $r_1 = -\frac{\pi^2}{2n^3}$. This indicates the gap opening from the electromagnetic field is small. Secondly, compared to other multilayer systems studied in the literature the flat band ATMG is more stable. Distinguished from ABC trilayer graphene stacked on hexagonal boron nitride or twisted double bilayer graphene, do not exhibit magic angles or flat bands when realistic effects, e.g., trigonal warping terms, are included. Most notably, we study the ATMG by decomposing it into several subsystems and find that the coupling of the laser field to the system is intra-subsystem and does not decay with the increasing layer number, which is more controllable than other techniques.

ACKNOWLEDGMENTS

This work is supported by the National Natural Science Foundation of China (Grant Nos. 12104099).

[1] Yuan Cao, Valla Fatemi, Ahmet Demir, Shiang Fang, Spencer L Tomarken, Jason Y Luo, Javier D Sanchez-Yamagishi, Kenji Watanabe, Takashi Taniguchi, Efthimios Kaxiras, et al. Correlated insulator behaviour at half-filling in magic-angle graphene superlattices. *Nature*, 556(7699):80–84, 2018.

[2] Yuan Cao, Valla Fatemi, Shiang Fang, Kenji Watanabe, Takashi Taniguchi, Efthimios Kaxiras, and Pablo Jarillo-Herrero. Unconventional superconductivity in magic-angle graphene superlattices. *Nature*, 556(7699):43–50, 2018.

[3] Matthew Yankowitz, Shaowen Chen, Hryhoriy Polshyn, Yuxuan Zhang, K Watanabe, T Taniguchi, David Graf, Andrea F Young, and Cory R Dean. Tuning superconductivity in twisted bilayer graphene. *Science*, 363(6431):1059–1064, 2019.

[4] Rafi Bistritzer and Allan H MacDonald. Moiré bands in twisted double-layer graphene. *Proceedings of the National Academy of Sciences*, 108(30):12233–12237, 2011.

[5] JMB Lopes Dos Santos, NMR Peres, and AH Castro Neto. Graphene bilayer with a twist: Electronic structure. *Physical review letters*, 99(25):256802, 2007.

[6] Aaron L Sharpe, Eli J Fox, Arthur W Barnard, Joe Finney, Kenji Watanabe, Takashi Taniguchi, MA Kastner, and David Goldhaber-Gordon. Emergent ferromagnetism near three-quarters filling in twisted bilayer graphene. *Science*, 365(6453):605–608, 2019.

[7] Ya-Hui Zhang, Dan Mao, and T Senthil. Twisted bilayer graphene aligned with hexagonal boron nitride: anomalous hall effect and a lattice model. *Physical Review Research*, 1(3):033126, 2019.

[8] Nick Bultinck, Eslam Khalaf, Shang Liu, Shubhayu Chatterjee, Ashvin Vishwanath, and Michael P. Zaletel. Ground state and hidden symmetry of magic-angle graphene at even integer filling. *Phys. Rev. X*, 10:031034, Aug 2020.

[9] Zhida Song, Zhijun Wang, Wujun Shi, Gang Li, Chen Fang, and B Andrei Bernevig. All magic angles in twisted bilayer graphene are topological. *Physical review letters*, 123(3):036401, 2019.

[10] Zhi-Da Song, Biao Lian, Nicolas Regnault, and B. Andrei Bernevig. Twisted bilayer graphene. ii. stable symmetry anomaly. *Phys. Rev. B*, 103:205412, May 2021.

[11] Biao Lian, Zhi-Da Song, Nicolas Regnault, Dmitri K. Efetov, Ali Yazdani, and B. Andrei Bernevig. Twisted bilayer graphene. iv. exact insulator ground states and phase diagram. *Phys. Rev. B*, 103:205414, May 2021.

[12] Ahmed Abouelkomsan, Zhao Liu, and Emil J Bergholtz. Particle-hole duality, emergent fermi liquids, and fractional chern insulators in moiré flatbands. *Physical review letters*, 124(10):106803, 2020.

[13] Cécile Repellin and T Senthil. Chern bands of twisted bilayer graphene: Fractional chern insulators and spin phase transition. *Physical Review Research*, 2(2):023238, 2020.

[14] Patrick Wilhelm, Thomas C Lang, and Andreas M Läuchli. Interplay of fractional chern insulator and charge density wave phases in twisted bilayer graphene. *Physical Review B*, 103(12):125406, 2021.

[15] Yonglong Xie, Andrew T Pierce, Jeong Min Park,

Daniel E Parker, Eslam Khalaf, Patrick Ledwith, Yuan Cao, Seung Hwan Lee, Shaowen Chen, Patrick R Forrester, et al. Fractional chern insulators in magic-angle twisted bilayer graphene. *Nature*, 600(7889):439–443, 2021.

[16] Christophe Mora, Nicolas Regnault, and B Andrei Bernevig. Flatbands and perfect metal in trilayer moiré graphene. *Physical review letters*, 123(2):026402, 2019.

[17] Tommaso Cea, Niels R Walet, and Francisco Guinea. Twists and the electronic structure of graphitic materials. *Nano letters*, 19(12):8683–8689, 2019.

[18] Ziyan Zhu, Stephen Carr, Daniel Massatt, Mitchell Luskin, and Efthimios Kaxiras. Twisted trilayer graphene: A precisely tunable platform for correlated electrons. *Physical review letters*, 125(11):116404, 2020.

[19] Yuncheng Mao, Daniele Guerci, and Christophe Mora. Supermoiré low-energy effective theory of twisted trilayer graphene. *Physical Review B*, 107(12):125423, 2023.

[20] Xianqing Lin, Cheng Li, Kelu Su, and Jun Ni. Energetic stability and spatial inhomogeneity in the local electronic structure of relaxed twisted trilayer graphene. *Physical Review B*, 106(7):075423, 2022.

[21] Zhen Ma, Shuai Li, Ming Lu, Dong-Hui Xu, Jin-Hua Gao, and XinCheng Xie. Doubled moiré flat bands in double-twisted few-layer graphite. *Science China Physics, Mechanics & Astronomy*, 66(2):227211, 2023.

[22] Zeyu Hao, AM Zimmerman, Patrick Ledwith, Eslam Khalaf, Danial Haie Najafabadi, Kenji Watanabe, Takashi Taniguchi, Ashvin Vishwanath, and Philip Kim. Electric field–tunable superconductivity in alternating-twist magic-angle trilayer graphene. *Science*, 371(6534):1133–1138, 2021.

[23] Ethan Lake and T. Senthil. Reentrant superconductivity through a quantum lifshitz transition in twisted trilayer graphene. *Phys. Rev. B*, 104:174505, Nov 2021.

[24] Wei Qin and Allan H MacDonald. In-plane critical magnetic fields in magic-angle twisted trilayer graphene. *Physical Review Letters*, 127(9):097001, 2021.

[25] Jeong Min Park, Yuan Cao, Li-Qiao Xia, Shuwen Sun, Kenji Watanabe, Takashi Taniguchi, and Pablo Jarillo-Herrero. Robust superconductivity in magic-angle multilayer graphene family. *Nature Materials*, 21(8):877–883, 2022.

[26] Yiran Zhang, Robert Polski, Cyprian Lewandowski, Alex Thomson, Yang Peng, Youngjoon Choi, Hyunjin Kim, Kenji Watanabe, Takashi Taniguchi, Jason Alicea, et al. Promotion of superconductivity in magic-angle graphene multilayers. *Science*, 377(6614):1538–1543, 2022.

[27] Patrick J Ledwith, Eslam Khalaf, Ziyan Zhu, Stephen Carr, Efthimios Kaxiras, and Ashvin Vishwanath. Tb or not tb? contrasting properties of twisted bilayer graphene and the alternating twist n-layer structures ($n = 3, 4, 5, \backslash \ldots$). *arXiv preprint arXiv:2111.11060*, 2021.

[28] Eslam Khalaf, Alex J Kruchkov, Grigory Tarnopolsky, and Ashvin Vishwanath. Magic angle hierarchy in twisted graphene multilayers. *Physical Review B*, 100(8):085109, 2019.

[29] Fedor K Popov and Grigory Tarnopolsky. Magic angles in equal-twist trilayer graphene. *arXiv preprint arXiv:2303.15505*, 2023.

[30] Guorui Chen, Aaron L Sharpe, Patrick Gallagher, Ilan T Rosen, Eli J Fox, Lili Jiang, Bosai Lyu, Hongyuan Li, Kenji Watanabe, Takashi Taniguchi, et al. Signatures of tunable superconductivity in a trilayer graphene moiré superlattice. *Nature*, 572(7768):215–219, 2019.

[31] Guorui Chen, Aaron L Sharpe, Eli J Fox, Ya-Hui Zhang, Shaoxin Wang, Lili Jiang, Bosai Lyu, Hongyuan Li, Kenji Watanabe, Takashi Taniguchi, et al. Tunable correlated chern insulator and ferromagnetism in a moiré superlattice. *Nature*, 579(7797):56–61, 2020.

[32] Ya-Hui Zhang, Dan Mao, Yuan Cao, Pablo Jarillo-Herrero, and T Senthil. Nearly flat chern bands in moiré superlattices. *Physical Review B*, 99(7):075127, 2019.

[33] Zhiyong Liu, Wenyuan Shi, Teng Yang, and Zhidong Zhang. Magic angles and flat chern bands in alternating-twist multilayer graphene system. *Journal of Materials Science & Technology*, 111:28–34, 2022.

[34] Bo Xie, Ran Peng, Shihao Zhang, and Jianpeng Liu. Alternating twisted multilayer graphene: generic partition rules, double flat bands, and orbital magnetoelectric effect. *npj Computational Materials*, 8(1):1–8, 2022.

[35] Xiaomeng Liu, Zeyu Hao, Eslam Khalaf, Jong Yeon Lee, Yuval Ronen, Hyobin Yoo, Danial Haei Najafabadi, Kenji Watanabe, Takashi Taniguchi, Ashvin Vishwanath, et al. Tunable spin-polarized correlated states in twisted double bilayer graphene. *Nature*, 583(7815):221–225, 2020.

[36] Jong Yeon Lee, Eslam Khalaf, Shang Liu, Xiaomeng Liu, Zeyu Hao, Philip Kim, and Ashvin Vishwanath. Theory of correlated insulating behaviour and spin-triplet superconductivity in twisted double bilayer graphene. *Nature communications*, 10(1):5333, 2019.

[37] Yuan Cao, Daniel Rodan-Legrain, Oriol Rubies-Bigorda, Jeong Min Park, Kenji Watanabe, Takashi Taniguchi, and Pablo Jarillo-Herrero. Tunable correlated states and spin-polarized phases in twisted bilayer–bilayer graphene. *Nature*, 583(7815):215–220, 2020.

[38] Cheng Shen, Yanbang Chu, QuanSheng Wu, Na Li, Shuopei Wang, Yanchong Zhao, Jian Tang, Jieying Liu, Jinpeng Tian, Kenji Watanabe, et al. Correlated states in twisted double bilayer graphene. *Nature Physics*, 16(5):520–525, 2020.

[39] Takashi Oka and Hideo Aoki. Photovoltaic hall effect in graphene. *Phys. Rev. B*, 79:081406, Feb 2009.

[40] Zhenghao Gu, H. A. Fertig, Daniel P. Arovas, and Assa Auerbach. Floquet spectrum and transport through an irradiated graphene ribbon. *Phys. Rev. Lett.*, 107:216601, Nov 2011.

[41] Takuya Kitagawa, Takashi Oka, Arne Brataas, Liang Fu, and Eugene Demler. Transport properties of nonequilibrium systems under the application of light: Photoinduced quantum hall insulators without landau levels. *Phys. Rev. B*, 84:235108, Dec 2011.

[42] Balázs Dóra, Jérôme Cayssol, Ferenc Simon, and Roderich Moessner. Optically engineering the topological properties of a spin hall insulator. *Phys. Rev. Lett.*, 108:056602, Jan 2012.

[43] Thomas Iadecola, David Campbell, Claudio Chamon, Chang-Yu Hou, Roman Jackiw, So-Young Pi, and Silvia Viola Kusminskiy. Materials design from nonequilibrium steady states: Driven graphene as a tunable semiconductor with topological properties. *Phys. Rev. Lett.*, 110:176603, Apr 2013.

[44] S. V. Syzranov, Ya. I. Rodionov, K. I. Kugel, and F. Nori. Strongly anisotropic dirac quasiparticles in irradiated graphene. *Phys. Rev. B*, 88:241112, Dec 2013.

[45] Motohiko Ezawa. Photoinduced topological phase transition and a single dirac-cone state in silicene. *Phys. Rev.*

Lett., 110:026603, Jan 2013.

[46] Arijit Kundu, HA Fertig, and Babak Seradjeh. Effective theory of floquet topological transitions. *Physical review letters*, 113(23):236803, 2014.

[47] Adolfo G Grushin, Álvaro Gómez-León, and Titus Neupert. Floquet fractional chern insulators. *Physical review letters*, 112(15):156801, 2014.

[48] Arijit Kundu, H. A. Fertig, and Babak Seradjeh. Floquet-engineered valleytronics in dirac systems. *Phys. Rev. Lett.*, 116:016802, Jan 2016.

[49] Mark S Rudner and Netanel H Lindner. Band structure engineering and non-equilibrium dynamics in floquet topological insulators. *Nature reviews physics*, 2(5):229–244, 2020.

[50] MA Sentef, M Claassen, AF Kemper, B Moritz, T Oka, JK Freericks, and TP Devereaux. Theory of floquet band formation and local pseudospin textures in pump-probe photoemission of graphene. *Nature communications*, 6(1):7047, 2015.

[51] Yantao Li, HA Fertig, and Babak Seradjeh. Floquet-engineered topological flat bands in irradiated twisted bilayer graphene. *Physical Review Research*, 2(4):043275, 2020.

[52] Christopher Yang, Iliya Esin, Cyprian Lewandowski, and Gil Refael. Optical control of slow topological electrons in moir\'e systems. *arXiv preprint arXiv:2301.02248*, 2023.

[53] Peng-Sheng Hu and Zhao Liu. Floquet fractional chern insulators and competing phases in twisted bilayer graphene. *arXiv preprint arXiv:2207.07314*, 2022.

[54] Michael Vogl, Martin Rodriguez-Vega, and Gregory A Fiete. Effective floquet hamiltonians for periodically driven twisted bilayer graphene. *Physical Review B*, 101(23):235411, 2020.

[55] Michael Vogl, Martin Rodriguez-Vega, and Gregory A Fiete. Floquet engineering of interlayer couplings: Tuning the magic angle of twisted bilayer graphene at the exit of a waveguide. *Physical Review B*, 101(24):241408, 2020.

[56] Patrick J. Ledwith, Grigory Tarnopolsky, Eslam Khalaf, and Ashvin Vishwanath. Fractional chern insulator states in twisted bilayer graphene: An analytical approach. *Phys. Rev. Res.*, 2:023237, May 2020.

[57] AB Kuzmenko, Iris Crassee, Dirk Van Der Marel, P Blake, and KS Novoselov. Determination of the gate-tunable band gap and tight-binding parameters in bilayer graphene using infrared spectroscopy. *Physical Review B*, 80(16):165406, 2009.

[58] Nicolas Leconte, Youngju Park, Jiaqi An, Appalakondaiah Samudrala, and Jeil Jung. Electronic structure of lattice relaxed alternating twist tng-multilayer graphene: from few layers to bulk at-graphite. *2D Materials*, 9(4):044002, 2022.